# *Spectral and spatial shaping of Smith-Purcell radiation*

PHYSICAL REVIEW A **96**, 061801(R) (2017)

# Spectral and spatial shaping of Smith-Purcell radiation

Roei Remez,[1,*] Niv Shapira,[1] Charles Roques-Carmes,[2] Romain Tirole,[2,3] Yi Yang,[2] Yossi Lereah,[1] Marin Soljačić,[2] Ido Kaminer,[2,4] and Ady Arie[1]

[1]*School of Electrical Engineering, Fleischman Faculty of Engineering, Tel Aviv University, Tel Aviv, Israel*
[2]*Research Laboratory of Electronics, Massachusetts Institute of Technology, Cambridge, Massachusetts 02139, USA*
[3]*Department of Physics, Faculty of Natural Sciences, Imperial College London, London SW7 2AZ, United Kingdom*
[4]*Department of Electrical Engineering, Technion–Israel Institute of Technology, Haifa 32000, Israel*

(Received 28 September 2017; published 6 December 2017)

The Smith-Purcell effect, observed when an electron beam passes in the vicinity of a periodic structure, is a promising platform for the generation of electromagnetic radiation in previously unreachable spectral ranges. However, most of the studies of this radiation were performed on simple periodic gratings, whose radiation spectrum exhibits a single peak and its higher harmonics predicted by a well-established dispersion relation. Here, we propose a method to shape the spatial and spectral far-field distribution of the radiation using complex periodic and aperiodic gratings. We show, theoretically and experimentally, that engineering multiple peak spectra with controlled widths located at desired wavelengths is achievable using Smith-Purcell radiation. Our method opens the way to free-electron-driven sources with tailored angular and spectral responses, and gives rise to focusing functionality for spectral ranges where lenses are unavailable or inefficient.

DOI: 10.1103/PhysRevA.96.061801

## I. INTRODUCTION

Ever since its first observation in 1953 [1], Smith-Purcell radiation (SPR) has been studied extensively, mainly due to its potential to generate light at hard-to-reach electromagnetic frequencies, such as the far-infrared, terahertz, and x-ray ranges [2–7]. This radiation, which originates from the collective oscillations of charges induced by free charged particles above a periodically patterned surface, is characterized by a specific dispersion relation and emission at every angle in the plane normal to the surface.

The community has explored various theories to account for the physics of this phenomenon in metallic gratings [8–11] and to increase the efficiency of the radiation [4–6,12]. Even more advanced theories revealing quantum features of this effect [13,14] assumed simple periodic structures, giving a momentum $n\frac{2\pi}{\Lambda}\vec{x}$ to the incoming electron (where $n$ and $\Lambda$ are the diffraction order and grating period, respectively). Recently, the study of SPR was extended beyond the simple periodic structure, into aperiodic arrays [15], disordered plasmonic arrays [16], and Babinet metasurfaces for manipulating the SPR polarization [17]. However, to the best of our knowledge, no attempt has been made to shape the angular spectrum and frequency spectrum of SPR.

In this Rapid Communication, we develop a systematic method for shaping the SPR's angular and frequency spectrum using complex periodic and aperiodic gratings. First, we show theoretically and experimentally that the single peak of the conventional SPR far-field distribution can be split into a desired set of peaks by properly designing a complex periodic grating, and demonstrate twin-peak and triple-peak shaping. We then discuss the advantages and limitations of the method and study the effect of the interaction length on the radiation, showing that it can be used to smoothen the spectral or angular response for a desired outcome. We conclude with a theoretical suggestion corroborated by a set of simulations for a Smith-Purcell cylindrical lens.

## II. THEORETICAL ANALYSIS OF SMITH-PURCELL RADIATION IN COMPLEX PERIODIC GRATINGS

We start with writing the expression of the field emitted from an infinite metallic periodic grating, positioned at the $(x,y)$ plane with the rulings parallel to the $y$ direction, and where the electron is passing close to the grating with velocity $v_0\hat{x}$, as proposed by Van den Berg [8],

$$E_x(x,y,z,t) = \frac{1}{2\pi^2}\mathrm{Re}\left[\int_0^\infty d\omega \int_{-\infty}^\infty d\beta \times \sum_{n=-\infty}^{\infty} \epsilon_{xn}^r(\beta,\omega) e^{i\alpha_n x + i\beta y + i\gamma_n z - i\omega t}\right], \quad (1)$$

where $\alpha_n = \frac{\omega}{v_0} + \frac{2\pi n}{\Lambda} = k_0 \sin\phi \sin\theta_n$, $\beta = k_0 \cos\phi$, $\gamma_n = \sqrt{k_0^2 - \beta^2 - \alpha_n^2}$, $k_0 = \frac{\omega}{c} = \frac{2\pi}{\lambda_0}$, $\lambda_0$ and $\omega$ are the vacuum wavelength of light and its angular frequency, $c$ is the velocity of light, $\phi$ is the angle of the wave vector with the $y$ axis, and $\theta_n$ is the angle of the projected $k$ vector on the $(x,z)$ plane with the $z$ axis (see Fig. 1). The discrete summation over $n$ originates from the different diffraction orders of the grating, with corresponding spatial frequency components $\alpha_n$ and $\gamma_n$. Although the summation is on all values of $n$, we note that for high diffraction orders $\gamma_n$ becomes imaginary and the wave is therefore evanescent. From the equation for $\alpha_n$ we can formulate the dispersion equation

$$\lambda_0 = \frac{\Lambda}{n}\left(\sin\phi \sin\theta_n - \frac{c}{v_0}\right), \quad (2)$$

which is equivalent to the dispersion relation from the first paper by Smith and Purcell [1]. Equation (1) represents decomposition into plane waves in the direction $(\theta_n,\phi)$.

*roei.remez@gmail.com.

 

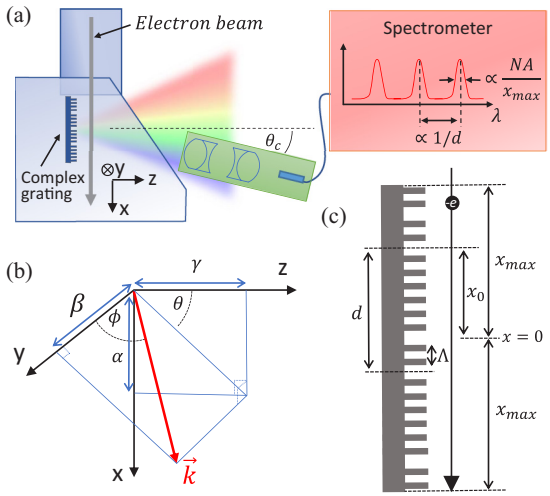


FIG. 1. Experimental setup. (a) The special grating was positioned inside the viewing chamber of the transmission electron microscope, while the output radiation is collected using lenses and a spectrometer located outside the microscope. Inset to (a): The spectral response of the first diffraction order of the radiation exhibits multiple peaks with spacing and width inversely proportional to the dislocation period and the interaction length, respectively. (b) Definition of angles and momentum components of the emitted light. $\phi$ is the angle between the wave vector of the emitted light and the $y$ axis, and $\theta$ is the angle between the projection of the $\vec{k}$ vector on the $xz$ plane and the $z$ axis. (c) Schematic drawing of a complex periodic grating, showing the supercell of period $d$ created by half-period spacings on an otherwise constant period $\Lambda$.

Defining $E_{xn}$ as the complex electric field of the $n$th diffraction order,

$$E_{xn} = \frac{1}{2\pi^2}\int_0^\infty d\omega \int_{-\infty}^{\infty} d\beta \epsilon_{xn}^r(\beta,\omega) e^{i\alpha_n x + i\beta y + i\gamma_n z - i\omega t},$$

we can approximate the electric field emitted in the case of a structured grating (SG) as

$$E_x^{\mathrm{SG}}(x,y,0,t) = \mathrm{rect}\left(\frac{x-x_0}{2x_{\max}}\right)\sum_{n=-\infty}^{\infty} f_n(x) E_{xn}(x,y,0,t), \quad (3)$$

where $2x_{\max}$ is the interaction length of the electron with the grating, $x_0$ is the center of the interaction with respect to an arbitrary point at the grating, and $f_n(x)$ denotes the effect of the deviation from a periodic grating on the electric field of the $n$th diffraction order at the grating's plane $z = 0$. We note that in a single SPR experiment, usually many values of $x_0$ are measured simultaneously, since the nonzero width of the electron beam gives different interaction areas for each electron.

To exemplify our method, we limit our derivation for the case of constant duty cycle (ridge to period ratio) of 50%, which results in phase-only changes for the electric field at $z = 0$. We can define a function $s(x)$ that expresses the structuring of the grating (the results below can be directly generalized to any duty cycle and even arbitrary grating shapes). A shift of $s(x)\Lambda$ in the groove position [where $0 \leqslant s(x) \leqslant 1$] will result in a phase shift $\Delta\psi_n$ for order $n$ of the electric field at $z = 0$, given by $\Delta\psi_n = 2\pi s(x)n$, where $n$ is the SPR diffraction order (see Ref. [18] for Huygens construction of this expression). Therefore, $f_n(x) = e^{i2\pi s(x)n}$. Here, the function $s(x)$ [and therefore $f_n(x)$] is assumed periodic of period $d$, however, as we discuss below, this does not have to be the case, and some interesting results can be achieved with nonperiodic variations of the grating. The electric field at the grating plane can be rewritten as a far-field expression, defining the far-field angular distribution $\eta_x^r(\alpha,\beta,\omega)$,

$$E_x^{\mathrm{SG}}(x,y,0,t) \equiv \frac{1}{2\pi^2}\int_0^\infty d\omega \int_{-\infty}^{\infty} d\beta \int_{-\infty}^{\infty} d\alpha \eta_x^r(\alpha,\beta,\omega) e^{i\alpha x + i\beta y - i\omega t}. \quad (4)$$

Comparing Eqs. (3) and (4), we get

$$\eta_x^r(\alpha,\beta,\omega) = 2x_{\max}\sum_{n=-\infty}^{\infty} e^{-i\alpha x_0}\epsilon_{xn}^r(\beta,\omega)\mathrm{sinc}\{[\alpha-\alpha_n(\omega)]x_{\max}\} \otimes \mathrm{FT}\{f_n(x)\},$$

where $\mathrm{FT}\{f_n(x)\}$ is the Fourier transform of $f_n(x)$, and $\otimes$ denotes convolution. Since $f_n(x)$ is periodic, we can write its Fourier transform as a Fourier series $\mathrm{FT}\{f_n(x)\} = \sum_{\mathrm{m}=-\infty}^{\infty} a_{mn}\delta(\alpha - \frac{2\pi m}{d})$, where $d$ is the period of $f_n(x)$ and $a_{mn}$ are Fourier coefficients,

$$a_{mn} = \frac{1}{d}\int_d e^{i2\pi s(x)n} e^{i2\pi m x/d} dx. \quad (5)$$

Finally, the angular far-field expression is given by

$$\eta_x^r(\alpha,\beta,\omega) = 2x_{\max}\sum_n \epsilon_{xn}^r(\beta,\omega)\sum_m a_{mn} e^{-i(\alpha-\frac{2\pi m}{d})x_0}\mathrm{sinc}\left[\left(\alpha - \frac{2\pi m}{d} - \alpha_n\right)x_{\max}\right], \quad (6)$$

where $2x_{\max}$ is the interaction length of the electron with the grating, and $x_0$ is the position of the interaction area with respect to an arbitrary point in the grating. If the optical collecting system has a finite aperture $\xi$, centered around angular coordinates $(\theta,\phi) = (\theta_c,\pi/2)$, the measured power for each angular frequency $\omega$ will be proportional to the

integration of the intensity of that frequency over the collecting aperture,

$$P(\omega) \propto \iint_{\xi} \left|\eta_x^r(\alpha,\beta,\omega)\right|^2 d\alpha\, d\beta. \tag{7}$$

For a small collecting aperture with angular diameter $A < \frac{2\pi}{dk_0}$ and an interaction length larger than the period of the variation, $2x_{\max} > d$, Eqs. (6) and (7) give a spectrum with a series of separated peaks. The peaks are centered at wavelengths $\lambda_{mn}$ yielding (for $\phi = \pi/2$)

$$\lambda_{mn} = \frac{\sin\theta_c - \frac{c}{v_0}}{\frac{n}{\Lambda} + \frac{m}{d}}. \tag{8}$$

The expression is identical to the ordinary SPR equation [Eq. (2)] for the zeroth order $m = 0$, but for $m \neq 0$, additional peaks appear in different locations which are determined by the variation periodicity $d$. Interestingly, the zeroth-order amplitude $a_{0n}$ can be canceled, eliminating the original SPR peak, by adequately designing the structuring function $s(x)$ so the phase $e^{i\Delta\psi}$ averages to zero (as in Fig. 2). The width of the peaks is set by the interaction length $2x_{\max}$ and by the aperture of the collection system. Increasing the aperture $A$, or decreasing the interaction length $2x_{\max}$ (as in Fig. 3), widens the spectral peaks while their central wavelength remains constant, until the peaks become inseparable. Since it is assumed that each electron has a different value of $x_0$, the radiation from different electrons is summed incoherently with an equal distribution of $x_0$ between 0 and $d$.

## III. SPECTRAL SHAPING OF SPR

Figure 2 demonstrates the modification of the first diffraction order ($n = -1$) of SPR using structures with a half-period shift every $M/2$ periods of the grating, therefore $d = (M+1)\Lambda$. For example, see Fig. 2(a) for a schematic grating illustration when $M = 16$ ($\Lambda = 400$ nm for all gratings). The phase of the emitted light is zero for $M/2$ periods, then $\pi$ for $M/2$ periods, then zero again for $M/2$ periods, and so on. Therefore, the emitted light has a phase periodicity of $(M+1)$ periods, when the $+1$ is needed because of the two half-period shifts. In this case, the two dominant Fourier coefficients in Eq. (5) are $a_1$ and $a_{-1}$, as shown in Fig. 2(b), where we have omitted the $n$ subscript $a_m \equiv a_{m,n=-1}$. Importantly, this nulls the zeroth-order Fourier coefficient $a_0$, which defines the amplitude of the original SPR diffraction expression [Eq. (2)]. For these types of $s(x)$ functions we therefore expect the original SPR spectral peak of the $n = -1$ order to be zero.

The gratings for the experiments in this Rapid Communication were fabricated using electron beam lithography on a 500-$\mu$m BK7 substrate, coated with 200 nm silver, and resulting in a groove height of another 190 nm of silver and about 50% duty cycle. The gratings were placed inside the viewing chamber of an FEI-Technai 200-keV electron microscope, and were aligned to be almost parallel to the electron beam. The optical setup outside the microscope's viewing chamber consisted of two 2-in. doublet lenses, chromatically corrected for the measured spectral range, and a collecting fiber, connected to an Avantes ULS2048L spectrometer with a spectral resolution of 1.4 nm [see Fig. 1(a)]. A circular aperture of 13 mm, placed 27 cm from the grating, was used to limit the angular acceptance of the light collection system in all the experiments in this work, therefore the full acceptance angle was 48 mrad.

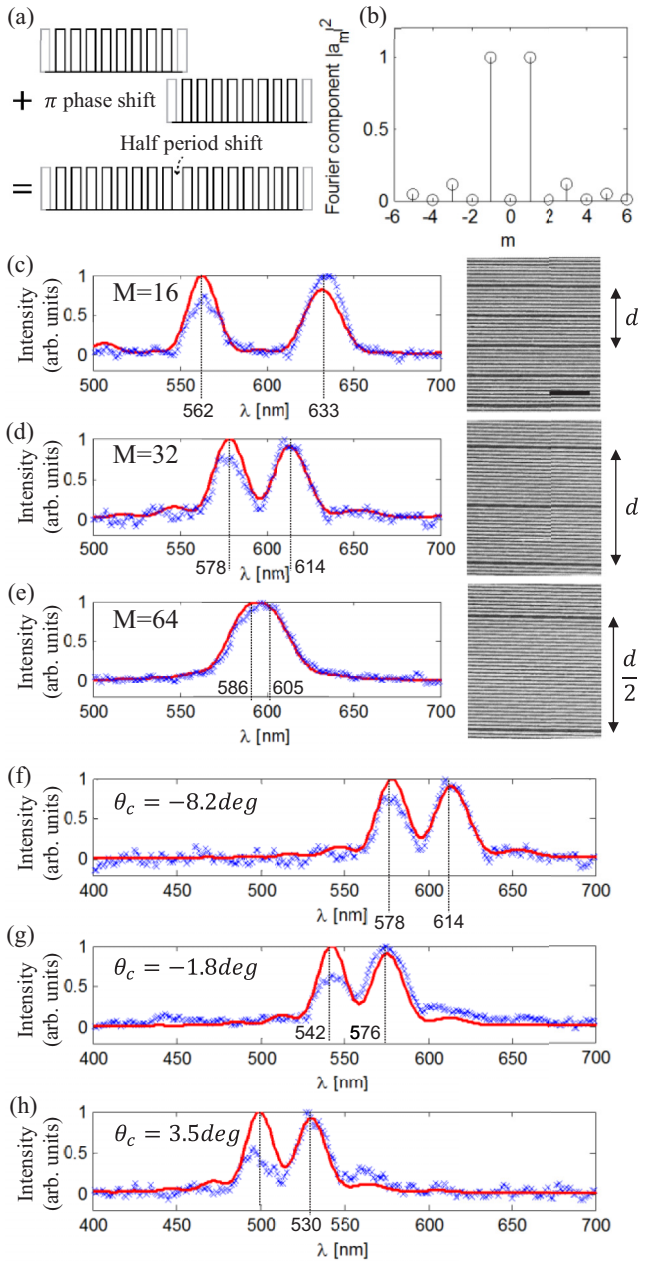


FIG. 2. Spectral splitting of Smith-Purcell peak. (a) Schematic demonstration of half-period shift. (b) The Fourier components of the phase function, showing two main peaks of the $\pm 1$ orders and a suppressed zero order. (c)–(h) Theoretical [according to Eq. (7), solid red] and experimental (blue $\times$'s) Smith-Purcell radiation spectrum for twin-peak designs. Marked: Peak locations according to Eq. (8), for $m = \pm 1$. (c)–(e) Spectral response for $\theta_c = -8.2^\circ$, for different $M$ values. $\Lambda = 400$ nm for all three gratings. Insets to (a)–(c): Scanning electron microscope images of the gratings used for (c)–(h); the scale bar is 5 $\mu$m. (f)–(h) Spectral response for the grating of $M = 32$, for different $\theta_c$ values.

The experimental and theoretical spectral responses for different $M$ values are given in Figs. 2(c)–2(e). The twin-peak spectral shape is clearly visible for $M = 16$ [Fig. 2(c)]. When

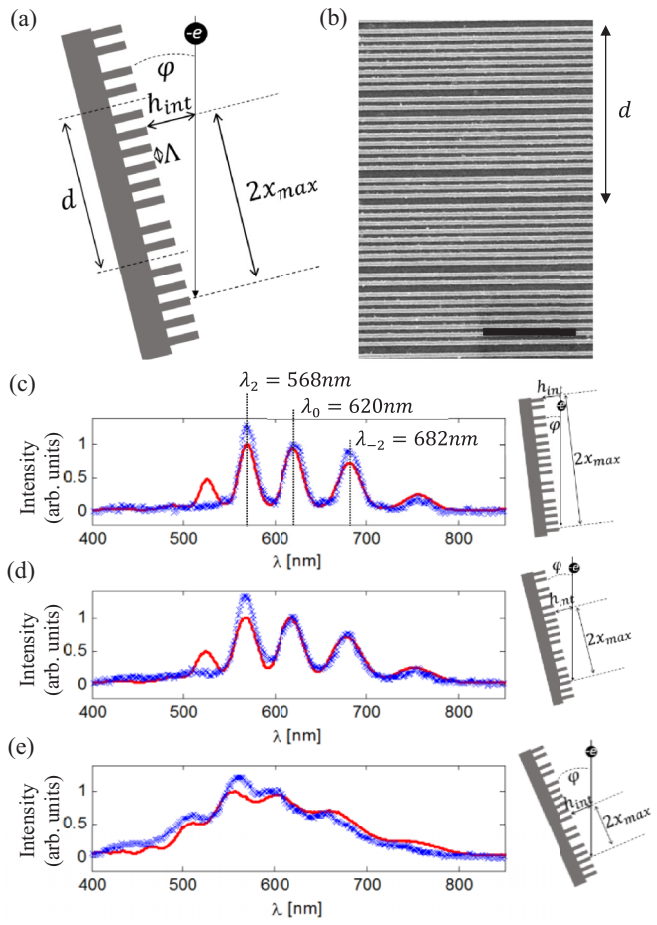


FIG. 3. Influence of the interaction length on spectral shaping. (a) Schematic drawing showing the change of interaction length caused by varying the angle between the electron beam and the grating. (b) Scanning electron microscope image of grating for the five-peak design. Scale is 5 $\mu$m. (c)–(f) Theoretical [according to Eq. (7), solid red] and experimental (blue $\times$'s) Smith-Purcell radiation spectrum for three-peak design, for different interaction lengths, changed by altering the angle between the electron beam and the grating. Marked: Wavelengths $\lambda_m = \lambda_{m,n=-1}$ according to Eq. (8).

$M$ increases, the two peaks get closer to one another, until for $M = 64$ [Fig. 2(e)] they are no longer separated, because of the limited interaction distance that depicts the number of unit cells ($\sim$30) that the electron is interacting with. By optimizing the first of the measured widths to simulation, we estimate the value for the interaction length to be 12 $\mu$m. Using this value alone, our theory shows a very good fit to all spectra [red curves in Figs. 2(c)–2(e)]. Figures 2(c)–2(e) were taken for the same value of $\theta_c$ which we measure to be $-7.7^\circ \pm 1.5^\circ$, close to $-8.2^\circ$ that optimizes the fit of theory and experiments.

Figures 2(f)–2(h) present the same grating of Fig. 2(d) for different collecting angles $\theta_c$, showing that the main effect of changing the angle of collection is the wavelength translation of the response, much as in regular SPR. Therefore, the far-field distribution of a single wavelength also maintains a twin-peak angular distribution. We note that the difference between the theoretical and the experimental curves is the result of the assumption that $\epsilon^r_{xn}(\beta,\omega)$ is constant for different light frequencies. The presented optimized values of $\theta_c$ [$-8.2^\circ$, $-1.8^\circ$, and $3.5^\circ$ for Figs. 2(f)–2(h)] are well inside the error range ($\pm 1.5^\circ$) of the measured values ($-7.7^\circ$, $-1.2^\circ$, and $2.2^\circ$, respectively).

Efficient SPR emission by the electrons is only possible when the electron passes in proximity to the grating surface within the interaction range ($z < h_{\text{int}}$). The $\omega$ component of the electrostatic field of an electron of velocity $v$ decays transversely within a range [3,9] $h_{\text{int}} \approx \tilde{\beta}\tilde{\gamma}\lambda/4\pi$, where $\tilde{\beta} = v_0/c$ and $\tilde{\gamma} = (1-\tilde{\beta}^2)^{-0.5}$. In our case, $\tilde{\beta} = 0.7$, and for small $\theta$ values ($\lambda \approx \frac{\Lambda}{\tilde{\beta}} = 0.57\,\mu$m) this corresponds to $h_{\text{int}} \approx 45$ nm. We note that the estimation of $h_{\text{int}}$ is used later only to approximate the experimental beam alignment capabilities, as we concentrate on shaping the emitted radiation rather than predicting the radiation energy.

The finite interaction length limits our spectral control, as is apparent from Fig. 2(e), where the two peaks merge into a single wider peak. The limited interaction length in our experiments is the result of the angle between the electron beam and the grating, marked as $\varphi$ in Fig. 3(a). Ideally, this angle would be zero, however, the width of the electron beam and alignment limitations in our setup prevent us from achieving perfect parallelism. Interestingly, we can also use this angle degree of freedom to our advantage when a wider-spectrum source is desired: Increasing $\varphi$ causes the peaks to widen and creates a smoother spectrum due to the smaller interaction length. To investigate this further we use a grating design [Fig. 3(b)] that exhibits a triple-peak response (the $-2$, 0, and $+2$ Fourier coefficients; see Ref. [18] for the design of this grating). Figure 3(c) presents the measured spectrum using the same aperture and $\Lambda$ values as the previous experiment, along with a theoretical curve to which the interaction length was fitted to be 10 $\mu$m (or $25\Lambda$). A beam angle or beam angular spread of about 5 mrad can cause such a coherence length limit, considering the estimated value of $h_{\text{int}} = 45$ nm. Deliberately increasing the angle $\varphi$ between the electron beam and the grating decreases the interaction length and widens the spectral peaks [Figs. 3(d) and 3(e)]. This confirms the interpretation of SPR as a coherent diffraction effect to which each unit cell is contributing. Note that the collection angle $\theta_c$ is effectively shifted by $\varphi$ (even when the collection system in the laboratory remains fixed). The values after optimization for Figs. 3(c), 3(d), and 3(e) were $\theta_c = -7^\circ$, $-6.7^\circ$, and $-4.8^\circ$, while $2x_{\text{max}} = 10$, 7, and 4.6 $\mu$m, respectively.

## IV. SPATIAL SHAPING OF SPR

The concepts we outlined above further enable one to investigate ways to shape the spatial response of SPR. For instance, we propose here a general design for a "Smith-Purcell lens" that will focus the emitted radiation at a predesigned point in the $(x,z)$ plane. This way the SPR source will multiplex the functionality of the source and the lens, which for certain spectral ranges (e.g., extreme ultraviolet) may be inefficient or nonexistent. A lens designed for wavelength $\lambda_c$ ($k_c = 2\pi/\lambda_c$) with focal length $f_{\text{len}}$, focused to an off-axis point with angle $\zeta$ with the $z$ axis, as illustrated in Fig. 4, requires a phase modulation of the form

$$\Delta\psi = k_c\sqrt{f_{\text{len}}^2 - x^2} + k_c x \sin\zeta.$$

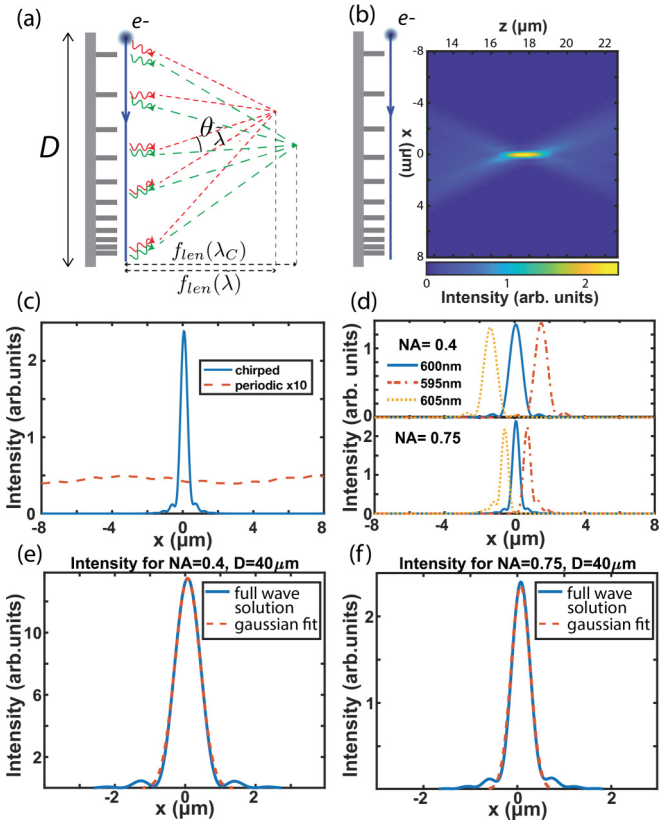


FIG. 4. Spatial shaping of SPR: design of a Smith-Purcell lens. (a) Schematic description of Smith-Purcell "cylindrical lens," designed to focus a wavelength $\lambda_c$ at focal distance $f_{\rm len}(\lambda_c)$ and suffering a chromatic aberration for other wavelengths. (b) Far-field radiation full-wave simulation as a function of the distance from the chirped grating. The length of the surface is $D = 40\,\mu$m (giving NA = 0.75), the acceleration voltage is 20 keV, and the focused wavelength $\lambda_c = 600$ nm. (c) Comparison chirped-grating far-field radiation in the focal plane, with a grating of constant period $\Lambda = 163$ nm (same as the average period of the chirped grating, the intensity being multiplied by ten to appear on the same scale). (d) Far-field radiation of multiple wavelengths in the focal plane with NA = 0.4 (top), NA = 0.75 (bottom). (e), (f) Intensity profile in the focal plane for (e) NA = 0.4 and (f) NA = 0.75. In (e) [(f)], the measured full width at half maximum (using Gaussian fit) is 855 nm (470 nm), compared to a diffraction-limited performance of 750 nm (400 nm).

Therefore, the angle of the emitted radiation from point $x$ on the grating should be $\sin\theta_n = \frac{1}{k_c}\frac{d(\Delta\psi)}{dx}$. From Eq. (2) we get (for $\phi = \pi/2$)

$$\Lambda(x) = \frac{n\lambda_c}{\frac{x}{\sqrt{f_{\rm len}^2 - x^2}} + \sin\zeta - \frac{c}{v_0}} \approx \frac{n\lambda_c}{\frac{x}{f_{\rm len}} + \sin\zeta - \frac{c}{v_0}}.$$

This result can also be explained using the shift function $s(x)$ notation, as we show in the Supplemental Material [18]. We note that the convergence exists only at the $x$-$z$ plane, and the divergence at the $y$-$z$ plane is left unchanged. Therefore, this device functions as a cylindrical lens to the emitted radiation.

In order to further explore this device, we used time-domain simulations using the commercial finite-difference time-domain (FDTD) software LUMERICAL. The electron beam can be represented as a time-dependent propagating point electron, $J(\vec{r},t) = -e\,v\,\delta(x - vt)\delta(y - y_0)\delta(z - z_0)$, and the associated polarization is $P(\vec{r},\omega) = i\frac{e}{\omega}\exp(-i\frac{\omega x}{v})\,\delta(y - y_0)\delta(z - z_0)\,\vec{x}$. We model the electron beam by a set of closely spaced dipole sources, in order to induce a polarization similar to $P(\vec{r},\omega)$. As can be seen in Fig. 4(c), a chirped grating focuses the emitted radiation for wavelength $\lambda_c$. If another wavelength $\tilde{\lambda}$ is used other than the design wavelength $\lambda_c$, we will get (for $x \ll f_{\rm len}$ and $\zeta = 0$)

$$\sin\theta = \frac{\tilde{\lambda}n}{\Lambda(x)} + \frac{c}{v_0} = \frac{x}{\frac{\lambda_c}{\tilde{\lambda}}f_{\rm len}} + \left(1 - \frac{\tilde{\lambda}}{\lambda_c}\right)\frac{c}{v_0}.$$

Therefore, wavelength $\tilde{\lambda}$ will have a different focal length, given by $\tilde{f}_{\rm len} = \frac{\lambda_c}{\tilde{\lambda}}f_{\rm len}$. The rightmost term is the tilt expected for wavelength $\tilde{\lambda}$ at $x = 0$, and gives the angle $\theta_{\tilde{\lambda}}$ between the center of the converging cone of each wavelength, $\sin\theta_{\tilde{\lambda}} = (1 - \frac{\tilde{\lambda}}{\lambda_c})\frac{c}{v_0}$. This spectral behavior is demonstrated in Figs. 4(a) and 4(d). We observe in our simulations [Figs. 4(e) and 4(f)] a focusing performance of 11.4% (17.5%) above the diffraction limit for numerical aperture NA = 0.4(NA = 0.75). See Ref. [18] for a further spectral and diffraction analysis of such a lens.

We conclude that this cylindrical-lens-like device has a strong axial chromatic dispersion, and the expected lateral chromatic dispersion of ordinary SPR. The high chromaticity of this device would be of interest for applications where a small bandwidth is required (deep UV lithography, mask inspection, and biological applications [19–21]) and spectrometry. Even though there has not been, to the best of our knowledge, any experimental demonstration of Smith-Purcell radiation in the deep ultraviolet so far, there are promising theoretical predictions in the literature [22,23], paving the way to an efficient, tunable source in the ultraviolet.

The highly dispersive nature of a Smith-Purcell lens shown in Fig. 4(d) would make the experimental demonstration of its close-to-diffraction-limited behavior challenging, at least with conventional broadband imaging systems (for instance, CCD cameras). This limitation could be circumvented by designing chirped metasurfaces made of resonators with a very high spectral quality factor or plasmon-locked SPR as has been recently proposed [24]. The latter approach relies on phase matching the plasmon dispersion relation with the electron beam line $\omega = kv$, thus preventing applications to extreme UV regimes. Other dispersion engineering tricks should also be investigated from, for instance, the field of achromatic metasurfaces [25].

## V. CONCLUSIONS

In this Rapid Communication, we have demonstrated how Smith-Purcell radiation can be shaped to a desired spectral or angular far-field response. Its resolution is limited only by the interaction length of the electrons with the modified grating. By carefully engineering the grating modulation function $s(x)$, and the resulting Fourier components $a_{nm}$ from Eq. (5), it is possible to create a light source with an arbitrary spectral and angular shape, at spectral ranges that are unreachable with conventional light sources. While most research in this field so far dealt with simple periodic gratings, for which the spectral

and angular response have a single peak [whose location is given by the ordinary Smith-Purcell dispersion Eq. (2) [1]], our method enables shaping the radiation spectrum into arbitrary line shapes, exemplified by our measured dual- and triple-peaked spectra. Furthermore, the method is not limited to periodic phase manipulations, and as we suggested one can use it to create a lens for a specific emitted wavelength, converging the beam in the $x$-$z$ plane. This might be useful for spectral ranges where lenses are hard to achieve, such as the UV or x-ray ranges [7].

We note that although the interaction length seems to impose a limitation on the widths of the peaks, the concept of superoscillations [26,27] might be used together with our method to achieve peaks at arbitrary small widths (with a penalty to the emitted intensity). The concepts of holography [28] can be used to design the structuring function $s(x)$ for shaping the complex Smith-Purcell emitted wave form (as was already demonstrated for transition radiation [29]). This can be achieved for example by varying other parameters of the grating structure such as the duty cycle, the ridge height, or the profile shape of the periods. Furthermore, in our theoretical analysis the value of $\epsilon^r_{xn}(\beta,\omega)$ is assumed constant, which explains the deviation of the peaks height from the theoretical curves. Therefore, this approach might be used to measure the function $\epsilon^r_{xn}(\beta,\omega)$ at a single spectral measurement.

## ACKNOWLEDGMENTS

The authors would like to thank Dr. Yigal Lilach and Roy Shiloh for assistance in fabrication, and Professor Avi Gover for stimulating discussions. This work was supported by DIP, the German-Israeli Project cooperation, by the Israel Science Foundation, Grant No. 1310/13, and by the US Army Research Office through the Institute for Soldier Nanotechnologies (Contract No. W911NF-13-D-0001). I.K. was supported by the FP7-Marie Curie International Outgoing Fellowship (IOF) under Grant No. 328853-MC-BSiCS.

[1] S. J. Smith and E. M. Purcell, Visible Light from Localized Surface Charges Moving across a Grating, Phys. Rev. **92**, 1069 (1953).

[2] A. Gover and Z. Livni, Operation regimes of Cerenkov-Smith-Purcell free electron lasers and T.W. amplifiers, Opt. Commun. **26**, 375 (1978).

[3] A. Gover and P. Sprangle, A unified theory of magnetic bremsstrahlung, electrostatic bremsstrahlung, Compton-Raman scattering, and Cerenkov-Smith-Purcell free-electron lasers, IEEE J. Quantum Electron. **17**, 1196 (1981).

[4] L. Schächter and A. Ron, Smith-Purcell free-electron laser, Phys. Rev. A **40**, 876 (1989).

[5] J. Urata, M. Goldstein, M. F. Kimmitt, A. Naumov, C. Platt, and J. E. Walsh, Superradiant Smith-Purcell Emission, Phys. Rev. Lett. **80**, 516 (1998).

[6] S. E. Korbly, A. S. Kesar, J. R. Sirigiri, and R. J. Temkin, Observation of Frequency-Locked Coherent Terahertz Smith-Purcell Radiation, Phys. Rev. Lett. **94**, 054803 (2005).

[7] M. J. Moran, X-ray Generation by the Smith-Purcell Effect, Phys. Rev. Lett. **69**, 2523 (1992).

[8] P. M. Van den Berg, Smith-Purcell radiation from a point charge moving parallel to a reflection grating, J. Opt. Soc. Am. **63**, 1588 (1973).

[9] J. H. Brownell, J. Walsh, and G. Doucas, Spontaneous Smith-Purcell radiation described through induced surface currents, Phys. Rev. E **57**, 1075 (1998).

[10] A. P. Potylitsyn, Resonant diffraction radiation and Smith-Purcell effect, Phys. Lett. A **238**, 112 (1998).

[11] A. Gover, P. Dvorkis, and U. Elisha, Angular radiation pattern of Smith-Purcell radiation, J. Opt. Soc. Am. B **1**, 723 (1984).

[12] S. L. Chuang and J. A. Kong, Enhancement of Smith-Purcell radiation from a grating with surface-plasmon excitation, J. Opt. Soc. Am. A **1**, 672 (1984).

[13] S. J. Glass and H. Mendlowitz, Quantum theory of the Smith-Purcell experiment, Phys. Rev. **174**, 57 (1968).

[14] S. Tsesses, G. Bartal, and I. Kaminer, Light generation via quantum interaction of electrons with periodic nanostructures, Phys. Rev. A **95**, 013832 (2017).

[15] J. R. M. Saavedra, D. Castells-Graells, and F. J. García de Abajo, Smith-Purcell radiation emission in aperiodic arrays, Phys. Rev. B **94**, 035418 (2016).

[16] I. Kaminer, S. E. Kooi, R. Shiloh, B. Zhen, Y. Shen, J. J. López, R. Remez, S. A. Skirlo, Y. Yang, J. D. Joannopoulos, A. Arie, and M. Soljačić, Spectrally and Spatially Resolved Smith-Purcell Radiation in Plasmonic Crystals with Short-Range Disorder, Phys. Rev. X **7**, 011003 (2017).

[17] Z. Wang, K. Yao, M. Chen, H. Chen, and Y. Liu, Manipulating Smith-Purcell Emission with Babinet Metasurfaces, Phys. Rev. Lett. **117**, 157401 (2016).

[18] See Supplemental Material at http://link.aps.org/supplemental/10.1103/PhysRevA.96.061801 for Huygens construction of the phase shift expression, triple-peak grating design, and extension of theory and simulations of SPR lens.

[19] G. Dattoli, A. Doria, G. P. Gallerano, L. Giannessi, K. Hesch, H. O. Moser, P. L. Ottaviani, E. Pellegrin, R. Rossmanith, R. Steininger, V. Saile, and J. Wüst, Extreme ultraviolet (EUV) sources for lithography based on synchrotron radiation, Nucl. Instrum. Methods Phys. Res. Sect. A **474**, 259 (2001).

[20] M. Holler, M. Guizar-Sicairos, E. H. R. Tsai, R. Dinapoli, E. Müller, O. Bunk, J. Raabe, and G. Aeppli, High-resolution non-destructive three-dimensional imaging of integrated circuits, Nature (London) **543**, 402 (2017).

[21] A. Ghisaidoobe and S. Chung, Intrinsic tryptophan fluorescence in the detection and analysis of proteins: A focus on Förster resonance energy transfer techniques, Int. J. Mol. Sci. **15**, 22518 (2014).

[22] F. J. García de Abajo, Interaction of Radiation and Fast Electrons with Clusters of Dielectrics: A Multiple Scattering Approach, Phys. Rev. Lett. **82**, 2776 (1999).

[23] Y. Yang, A. Massuda, C. Roques-Carmes, S. E. Kooi, T. Christensen, S. G. Johnson, J. D. Joannopoulos, O. D. Miller, I. Kaminer, and M. Soljačić (unpublished).

[24] Y.-C. Lai, T. C. Kuang, B. H. Cheng, Y.-C. Lan, and D. P. Tsai, Generation of convergent light beams by using surface plasmon locked Smith-Purcell radiation, Sci. Rep. **7**, 11096 (2017).

[25] F. Aieta, M. A. Kats, P. Genevet, and F. Capasso, Multiwavelength achromatic metasurfaces by dispersive phase compensation, Science **347**, 1342 (2015).

[26] M. Berry, Faster than Fourier, in *Quantum Coherence and Reality, Celebration of the 60th Birthday of Yakir Aharonov*, edited by J. S. Anandan and J. L. Safko (World Scientific, Singpaore, 1994), pp. 55–65.

[27] R. Remez and A. Arie, Super-narrow frequency conversion, Optica **2**, 472 (2015).

[28] W. H. Lee, Binary computer-generated holograms, Appl. Opt. **18**, 3661 (1979).

[29] G. Li, B. P. Clarke, J.-K. So, K. F. MacDonald, and N. I. Zheludev, Holographic free-electron light source, Nat. Commun. **7**, 13705 (2016).